Passive Forces in Mammalian Skeletal Muscle: A Freely-Jointed and Worm-Like Chain

J. MUÑIZ[1], J. L. MARÍN[2], M. HUERTA[1], J. DEL RIO[1], A. LARIOS[1] AND X. TRUJILLO[1]

1 *Centro Universitario de Investigaciones Biomédicas, Universidad de Colima, Apdo. Postal No. 11, 28000 Colima, Colima, México*
2 *Centro de Investigación en Física, Universidad de Sonora, Apdo Postal 5-088 83190 Hermosillo, Sonora, México*

Abstract. The passive mechanical properties of whole muscle in active and non-active states are compared. The experimental results are presented as stress-strain curves, which are analyzed in the framework of the current theoretical background [viz. the freely-jointed chain model (FJCM) and the worm-like chain model (WLCM)] in a semi-quantitative fashion. This analysis shows that both models can explain the mechanical behavior of whole muscle in non-active state. In the active state, the presence of crossbridges alters the mechanical response, leading to a markedly different behavior, as expected. A discussion of the mechanisms involved and the interpretation of the parameters required for the fitting of the stress-strain curves is also presented.

Key words: Mammalian skeletal muscle — Passive forces — Freely-jointed model — Worm-like chain model

Introduction

Mammalian skeletal muscles can be characterized functionally as either slow or fast-twitch depending on the relative content of slow-twitch (type I) and fast-twitch (type IIA and IIB) fibres. Fibre types are identified and classified according to their contractile and metabolic characteristics (Brooke and Kaiser 1970; Peter et al. 1972). The plantaris muscle of the rat is a fast muscle, containing as it does about 85% of type IIA-B muscle fibres.

Skeletal muscles develop both active and passive tension. The first involves the hydrolysis of ATP following actomyosin interaction in the presence of Ca^{2+}. Passive

Correspondence to Prof Dr. M Huerta, CUIB, Universidad de Colima, Apdo. Postal No 11, 28000-Colima, Colima, Mexico E-mail huertam@cgic.ucol.mx

tension involves a strain on the sarcomeric structures, and the evidence indicates that passive tension derives from the connecting filaments (Magid and Law 1985; Wang et al. 1991). These filaments comprise 6-12 molecules of the protein titin (Whithing et al. 1989; Funatsu 1996), a protein that spans from the M line to the Z-disc (Fürst et al. 1988). It has been demonstrated that titin protein extracted from slow muscle fibres shows less mobility in SDS-PAGE (sodium dodecyl sulphate-polyacrylamide gel electrophoresis) than that extracted from fast muscle fibres (Wang et al. 1991; Horowits 1992).

The passive tension developed in muscle can be analyzed using stress-strain curves. Such curves are qualitatively similar for the whole muscle, the isolated muscle fibre, the skinned skeletal muscle fibre and the isolated titin molecule (Magid and Law 1985; Tskhovrebova et al. 1997). Degradation of titin by ionizing radiation (Horowits et al. 1986) or chemical methods (Funatsu et al. 1990; Wang et al. 1993) decreases both the resting tension and the magnitude of the passive tension.

The purpose of this work was to analyze the stress-strain curves obtained for a fast skeletal muscle (*m. plantaris*) in male Wistar rats from the perspective of the classic models used to describe the mechanical behavior of polymers. The passive tension values used to construct the stress-strain curves were obtained from muscles in a resting state (at optimal length, L_0) or in an active state (tetanus). The freely-jointed chain model (FJCM) and the worm-like chain model (WLCM) (Fixman and Kovac 1973; Flory 1989) are known to describe, at least qualitatively, the region of low forces in the stress-strain curves.

Materials and Methods

Animal care

Eight-week-old male Wistar rats (n = 12; 228±38 g), were housed in individual acrylic cages under natural environmental conditions (mean annual temperature 26.4 ± 2 °C; mean annual humidity 66 ± 12%, natural light/dark cycle). Food and water were provided *ad libitum*. The dietary composition (%) was: protein, 24; fat, 8; fibre, 4.5; carbohydrates, 39.3; moisture, 12; minerals, ash, and vitamins 12.2. Animal care and experimental procedures both complied with the recommendations in the Guide for Care and Use of Laboratory Animals issued by the National Institute of Health (No. 85-23, 1985).

Surgeryl and experimental conditions

Under sodium pentobarbital anesthesia (4.0–6.0 mg/100g, i.p.), the right *plantaris* muscle (n = 12) was carefully freed from the surrounding tissues, leaving its attachments to the bones and its blood supply unimpaired. The motor nerve was cut as far as possible from its entry into the muscle. During the surgery, saline solution was instilled to keep the tissues wet. A mark at the muscle-tendon junction was

used to measure length Using a dentist's drill, holes were drilled in the femur and the calcaneus bones that form the distal insertion of the plantaris muscle Before the bones were drilled, the length of the muscle (L_m) in complete foot flexion was measured (4 18±0 07 cm, $n = 5$) After separation of the drilled distal bone, the rat was transferred to a low compliance ($< 3\ \mu mg^{-1}$) recording apparatus A steel rod was passed through the hole in the femur, then anchored to a pair of posts to obtain a rigid fixing A steel chain with a hook at the end passed through the hole in the finger bones to a force transducer, which was mounted on a computer-controlled stepper motor The minimum step size was 2 5 μm and the minimum time between steps was 3 ms The motor nerve was placed on stimulating electrodes During the experiment, the body temperature was maintained at 37°C

Protocol

At several muscle lengths, isometric twitches were elicited by applying supramaximal stimuli to the motor nerve until the maximal amplitude corresponding to the optimal length (L_0) was obtained L_0 was then measured using calipers The mean L_0 was 3 70±0 14 cm ($n = 5$) The muscles were mechanically cycled between L_0 and L_m ten times The lengthening that occurred in the last cycles was used for the analysis At a steady level of tetanic tension, the muscles were lengthening/shortening by 6% of L_0 The lengthening phases were used for the analysis Each tetanus was elicited by a 3 s supramaximal stimulus train at 250 Hz The mean velocity of the deformation cycle was 1mm/s

Force was recorded using a FT-10 GRASS transducer wired to a cyberamp 380 and a data acquisition system (Axon Instruments, Inc) sampling at 100 Hz for cycling from L_0 and at 500 Hz for tetani

Mechanical analysis

The passive tension (FORCE) was used to construct the stress-strain curves The stress was calculated

$$\sigma = \frac{\text{FORCE}}{\text{CSA}} \tag{1}$$

The cross-sectional area (CSA) was calculated from the following equation

$$\text{CSA} = \frac{\text{MASS}}{L_f^* 1\ 056} \tag{2}$$

where L_f^* is the length at the end of the set of lengthening steps (in cm), weight is the muscle wet weight (in g) as obtained at the end of the experiment, and 1 056 g cm ^{3} is the muscle density The mean muscle mass was 0 40±0 02 g ($n = 5$) The experiments were made at room temperature ($t = 24$°C)

The strain (δ) for a given deformation cycle was obtained from

$$\delta = \frac{L_f - L_0}{L_0} \tag{3}$$

The deformation cycle values were averaged for muscles under similar experimental conditions. All values are presented as means ± standard error (S E.M).

Results

The insert in Fig. 1 shows typical *plantaris* muscle tetani corresponding to initial (i) and final control (f) tetani and to the tetanus in which the deformation cycle

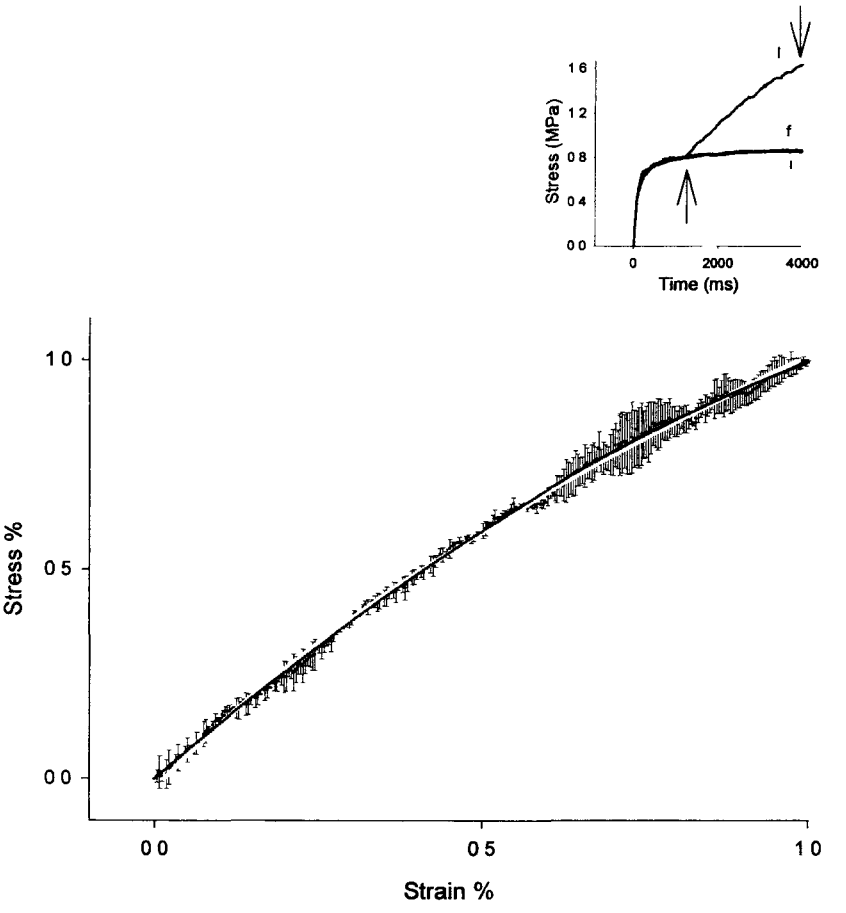

Figure 1. Stress-strain relationships for the mean tension in five *plantaris* muscles developed as a result of passive stretch during tetani The error bars represent S E M values The dotted curve represents Eq 9 (see the text) fitted to the experimental data The solid white curve represents Eq 8 (see the text) fitted to the experimental data The insert shows a typical experiment i is the initial control tetanus, f is the final control tetanus, and l is the tetanus in which the stretch was applied The tetani were terminated at the end of the stretch The arrows indicate the beginning and the end of the stretch

was applied (l). The records were terminated at the end of the lengthening phase. The value of the initial control tetanus was 1.02±0.08 MPa (n = 5) and that for the final control tetanus was 1.02±0.8 MPa (n = 5). The lengthening at a steady level of tetanus caused a tension development of 0.72±0.16 MPa (n = 5). The deformation cycles were each followed by a reduction in the steady level of active tension that always recovered by the end of the tetanus

The insert in Fig 2 shows examples of the passive tension elicited by de-

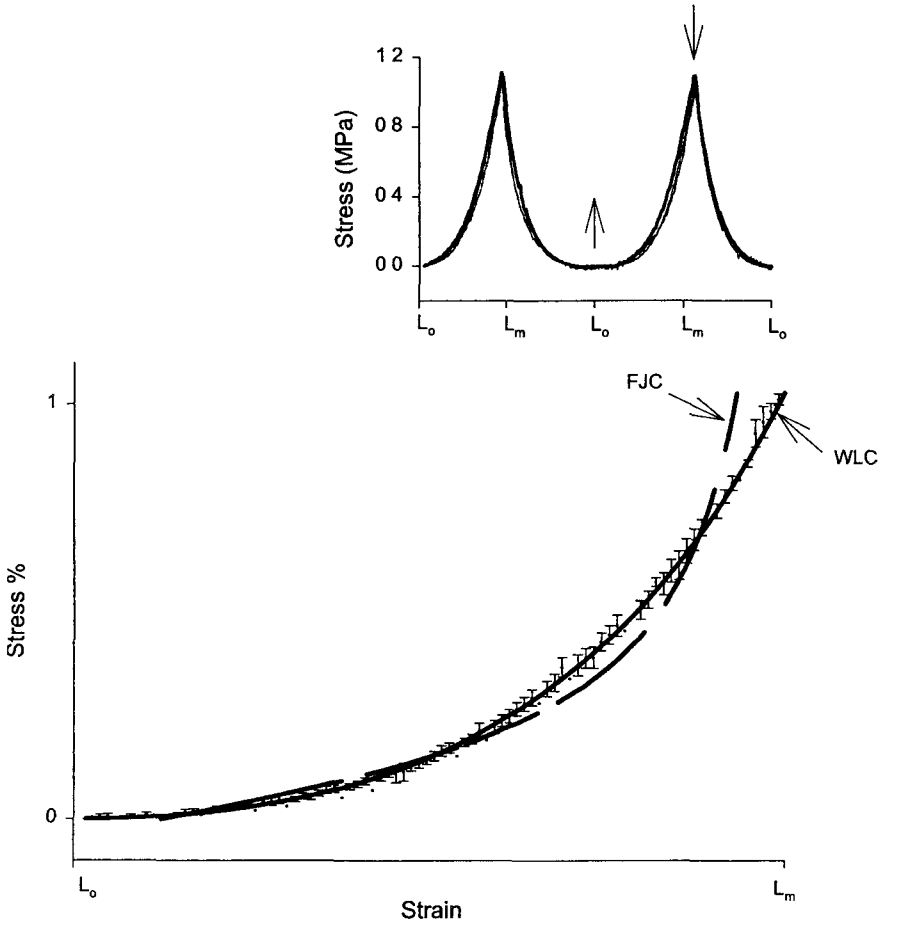

Figure 2. Stress-strain relationships for the mean tension in five *plantaris* muscles developed as a result of passive stretch from L_0 to L_m in non-active muscle The error bars represent S E M values WLC Eq 5 and FJC Eq 7 indicate fits to the experimental data The insert shows the stress-strain curves for the ninth and tenth deformation cycles in five *plantaris* muscles The ascending phase (between the arrows) was used for the analysis

formation cycles starting at L_0. The mean peak tension produced by the tenth deformation cycle was 0.9±0.2 MPa ($n = 5$).

The normalized passive tension is plotted in Figures 1 and 2 for the active and non-active states, respectively. In the case of the non-active state, the stress was measured from the basal tension at L_0. For the active state, the stress was measured from the steady tension level immediately preceding the deformation cycle.

Passive forces in the non-active state

In this section we will analyze the experimental results using the so-called freely-jointed chain model (FJC) and the worm-like chain model (WLC) (Fixman and Kovac 1973; Flory 1989; Higuchi et al. 1993; Wang et al. 1993). We used these models since the stress-deformation curves were obtained in the early stages of stretching [as also reported recently (Tskhovrebova et al. 1997) for a single titin filament from rabbit back skeletal muscle]. Both of these models can explain, at least qualitatively, the experimental results obtained so far.

In the FJC model, the length $\mathcal{L}$ of the titin filament and the external force f are related by:

$$\mathcal{L} = Nl\,[\coth(fl) - 1/fl] \tag{4}$$

where N is the number of β-domains; l is the persistence length; $f = F/\mathrm{k}T$; F being external force; k is the Boltzmann constant; and T is the temperature.

In view of the fact that the whole muscle contains a lot of such filaments, we can assume, qualitatively, that the strain and stress follow a similar relation, that is:

$$\delta = \delta_0\,[\coth(v) - 1/v] \tag{5}$$

where $v = \alpha(\sigma - \sigma_0)$ and α, σ_0 and δ_0 are parameters that can be obtained by fitting Eq. (5) to experimental results. The values for these parameters are $\alpha = 8.76$, $\sigma_0 = -0.04$, and $\delta_0 = 0.26$.

In the WLC model, the force F and the length x of the titin filament are related (Bustamante 1994) by:

$$F(x) = \mathrm{k}T/l\left\{\frac{1}{4}[1 - x/L]^{-2} - \frac{1}{4} + x/L\right\} \tag{6}$$

where k is the Boltzmann constant; T is the temperature, l is the persistence length, and L is the contour length.

As in the case of the FJC model, the stress and strain relationship for whole muscle can be assumed to be functionally similar to Eq. (6); in other words, their relationship can be expressed as:

$$\sigma = \sigma_0\left\{\frac{1}{4}[1 - \delta/\delta_0]^{-2} - \frac{1}{4} + \delta/\delta_0\right\} \tag{7}$$

where σ_0 and δ_0 are parameters that can be obtained by fitting experimental results to Eq (7) These parameters have the value of 1 24 and 0 53, respectively

In Fig 2, the best fit of the experimental data to Eqs (5) and (7) is depicted

Passive forces in the active state

In the case of the active state, it is clear that while the response of the muscle will be different, it will include in some way the contribution of the passive component If we assume that titin filaments behave the same as they do in the non-active state, then the relation between stress and strain would be

$$\delta = \delta_0[\coth(v) - 1/v] + \beta v^2 \tag{8}$$

In the case of the FJC model, the value of β is 3 03, α is -1 74, and δ_0 is -5 30, while

$$\sigma = \sigma_0 \left\{ \frac{1}{4}[1 - \delta/\delta_0]^{-2} - \frac{1}{4} + \delta/\delta_0 \right\} + \gamma(\delta/\delta_0)^{\frac{1}{2}} \tag{9}$$

In the case of the WLC model the parameters β and γ would represent the magnitude of the contribution made by the crossbridges to the mechanical response of the whole muscle The value of γ is 0 01, and those of δ_0 and σ_0 are 0 14 and -19 23, respectively

In Fig 1, the best fit of experimental data to Eqs (8) and (9) is depicted

Discussion

In the non-active state, the lack of crossbridges allows the entire passive response of the muscle to be attributed to the titin filaments, while in the active state (complete tetani) the presence of crossbridges involves the thin filaments and their connection with the Z-disc (see Fig 2) The lengthening during the plateau of tetani is known macroscopically as eccentric contraction

It is now clear that initial strain and stress, at the sarcomeric level, differ between the non-active and active states (in spite of the fact that the macroscopic length is almost unchanged), which explains the difference between the fitting parameters involved for the two states

We assumed that in the active state, the contribution made by the crossbridges to the passive response of the muscle is simply added to that originating from the titin filaments In this context, the area between the curves for the active and non-active states would correspond to the heat generated by the muscle as a product of the crossbridge working cycle The functional behavior of the contribution made by the active state in the FJC or the WLC is expressed through parameters β and γ in Eqs (8, 9)

Thus, a portion of the difference between the values of the fitting parameters can be attributed to the fact that in the active state, heat "spots" are produced

along the sarcomere as a result of ATP hydrolysis and the unfolding of the β-sheet domains (Erickson 1997; Jülicher et al. 1997).

At L_0, the connecting filaments may exist in folded β-sheet domains, and the PEVK may be extended. In the active state, these domains and the PEVK adjusting their length without changing the tension toward the Z-line.

We should mention here that we have assumed that the connective tissue (including the tendon) is acting only as a passive tension transmitter in both the active and non-active states (Magid and Law, 1985; Kellermayer et al. 1997).

In conclusion, our analysis suggests that the FJCM and the worm-like chain model can each explain, at least in a semi-quantitative way, the mechanical properties of whole muscle in both active and non-active states. There is a need to perform experiments to elucidate the changes that occur either in the persistence length or in the temperature at the filament level.

Acknowledgements. This research was supported by CONACyT, Mexico (grant No 1898PM & 29474N) to J Muñiz J D R and A L were CONACyT fellows

References

Brooke M H , Kaiser K K (1970) Muscle fibre types How many and what kind? Arch Neurol **23,** 369—379

Bustamante C (1994) Entropy elasticity of λ-phage DNA Science 265, 1599—1600

Erickson E P (1997) Stretching single protein molecules titin is a weird spring Science **276,** 1090—1092

Fixman M , Kovac J (1973) Polymer conformational statistics III Modified Gaussian models of stiff chains J Chem Phys **58,** 1564—1568

Flory P J (1989) Statistical Mechanics of Chain Molecules pp 304—316, (Hanser, Munich)

Funatsu T (1996) Elastic filaments in situ in striated muscle revealed by selective removal of the filaments with plasma gelsolin Adv Biophys **33,** 41—52

Funatsu T , Higuchi H , Ishiwata S (1990) Elastic filaments in skeletal muscle revealed by selective removal of thin filaments with plasma gelsolin J Cell Biol **110,** 53—62

Furst D O , Osborn M R , Weber N K (1988) The organization of titin filaments in the half-sarcomere revealed by monoclonal antibodies in immunoelectron microscopy, a map of ten nonrepetitive epitopes starting at the Z line extends close to the M line J Cell Biol **106,** 1563—1572

Higuchi H , Nakauchi Y , Maruyama K , Fujime S (1993) Characterization of b-connectin (titin 2) from striated muscle by dynamic light scattering Biophys J **65,** 1906—1915

Horowits R (1992) Passive force generation and titin isoforms in mammalian skeletal muscle Biophys J **61,** 392—398

Horowits R , Kempner E , Bisher M E , Podolsky R (1986) A physiological role for titin and nebulin in skeletal muscle Nature **323,** 160—164

Julicher F , Ajdari A , Prost J (1997) Modelling molecular motors Rev Mod Phys **69,** 1269—1281

Kellermayer M S Z , Smith S B , Granzier H L , Bustamante C (1997) Folding-unfolding transitions in single titin molecules characterized with laser tweezers Science **276,** 1112—1116

Magid A , Law D J (1985) Myofibrils bear most of the resting tension in frog skeletal muscle Science **230,** 1280—1282

Peter J B , Barnard R J , Edgerton V R , Gillespie C A , Stempel K E (1972) Metabolic profiles of three fibre types of skeletal muscle in guinea pig and rabbits Biochemistry USA **11,** 2627—2633

Tskhovrebova L , Trinick J , Sleep J A , Simmons R M (1997) Elasticity and unfolding of single molecules of the giant muscle protein titin Nature **387,** 308—312

Wang K , Wright J , Beverly J , Ramirez-Mitchell R (1991) Regulation of skeletal muscle stiffness and elasticity by titin isoforms a test of the segmental extension model of resting tension Proc Natl Acad Sci USA **88,** 7101—7105

Wang K , McCarter R , Wright J , Beverly J , Ramirez-Mitchell R (1993) Viscoelasticity of the sarcomere matrix of skeletal muscle the titin-myosin composite filament is a dual-stage molecular spring Biophys J **64,** 1161—1177

Whithing J , Wardak J , Trinick J (1989) Does titin regulate the length of muscle thick filaments? J Mol Biol **205,** 263—268

Final version accepted June 7, 1999